J Solid State Electrochem (2010) 14:681–686
DOI 10.1007/s10008-009-0828-z

ORIGINAL PAPER

The pH effects on the capacitive behavior of nanostructured molybdenum oxide

Hossein Farsi · Fereydoon Gobal · Heidar Raissi · Shokufeh Moghiminia

Received: 6 January 2009 / Revised: 3 March 2009 / Accepted: 6 March 2009 / Published online: 22 April 2009

Abstract Nanostructured molybdenum oxide having a particle size in the range of 30–80 nm was prepared by potentiodynamic electrodeposition method, and the effects of H_2SO_4 concentration on its capacitive behavior were studied by cyclic voltammetry, galvanostatic discharge, and electrochemical impedance spectroscopy. Poor to fair capacitive behaviors were witnessed depending on the electrolyte concentration and conditions of charge/discharge. Increasing acid concentration to 0.02 M had favorable effect, while beyond that, the effect was detrimental. Capacitance around 600 F g^{-1} was recorded in the potential range of 0 to −0.55 V vs. Ag/AgCl.

Keywords Molybdenum oxides · Nanostructure · Impedance spectroscopy · Capacitive behavior

Introduction

Transition metal oxides are suitable materials to host small ions like H^+ and Li^+ in intercalation/deintercalation processes, which makes them most demanded for a wide range of applications such as electrochromic and energy storage devices. Among metal oxides, molybdenum oxide seems to be a promising candidate for such applications due to its crystallographic structure and different oxidation states of molybdenum [1]. In fact, molybdenum oxide's interesting physical and chemical properties, including n-type semiconductivity, electrochromism, and reversible small ions storage, make it a potential material for catalysts [2], gas sensors [3,4], smart windows [5], and batteries [6–8] applications.

Among different methods for preparing molybdenum oxides, electrodeposition technique sounds to be the most economic and suitable for making thin films due to its lower energy consumption and good sticking of the film to a conducting supports. There are several reports on the synthesis of molybdenum oxides by electrodeposition method [9–15]. Also, potentiodynamic electrodeposition method has been widely used for making nanostructured metal oxides [16–19]. The recent researches on the electrochemical properties of molybdenum oxide has shown that these properties depend not only to the nature of electrolyte but also to the morphology and the thickness of the oxide film, for instance, Więcek and Twardoch have reported a maximum capacitance of around 0.1 F cm^{-2} for electrodeposited molybdenum oxides in 0.005 M H_2SO_4 [15], whereas Więcek and Kępas-Suwara have obtained a specific capacity of 160 F g^{-1} in 0.1 M K_2SO_4 solution [20] and Takasu et al. a comparable capacitance to RuO_2 of around 1,000 F g^{-1} at low loading amount (0.5 nmol cm^{-2}) of highly dispersed and nanosized molybdenum oxides [21].

In this study, we prepared nanostructured molybdenum oxide by potentiodynamic electrodeposition onto stainless steel and investigated the effects of pH on its capacitive behavior by cyclic voltammetery, galvanic charge/discharge, and impedance spectroscopy. Also, we studied the limitation in acid concentration by monitoring instabilities of molybdenum oxides and side reactions like hydrogen evolution reaction.

H. Farsi (✉) · H. Raissi · S. Moghiminia
Department of Chemistry, University of Birjand,
P. O. Box 97175-615, Birjand, Iran
e-mail: hofarsi@birjand.ac.ir

F. Gobal
Department of Chemistry, Sharif University of Technology,
P. O. Box 11365-9516, Tehran, Iran

Experimental

The preparation method of nanostructured molybdenum oxide has been reported in details elsewhere [22]. Briefly, the amorphous nanostructured molybdenum oxide was potentiodynamically electrodeposited onto the surface of commercial grade stainless steel, which had been polished with emery paper nos. 400 to 1200 to a rough finish, washed free of emery particles in dilute nitric acid solution, rinsed with water, and air-dried. Electrodeposition was carried out in a (0.01 M H_2SO_4 + 0.04 M Na_2MoO^4) solution in the potential range of 0.00 to −0.75 V vs. Ag/AgCl with the potential sweep rate of 300 mV s^{-1}. H_2SO_4 and Na_2MoO^4 were Merck products, and all solutions were prepared using double distilled water. Subsequent to deposition, the obtained electrode was washed in distilled water and then used in electrochemical test solution, which hereafter we will call it as-deposited nanostructured molybdenum oxide, ANMO.

Electrochemical studies were carried out in a conventional three-electrode cell where the (coated) stainless steel sheet, a platinum grid, and a saturated Ag/AgCl electrode were used as a working, counter, and reference electrodes, respectively.

Cyclic voltammetery and galvanic charge/discharge tests were performed by a Solartron Electrochemical interface SI1287. Electrochemical impedance spectroscopy studies were carried out by a Solartron Phase Gain Analyzer SI1260. The electrochemical tests were performed in solutions of 0.005, 0.010, and 0.020 M H_2SO_4 at room temperature, and for each solution, a fresh working electrode was employed.

The amount of molybdenum oxides in the film was measured by dissolving of the film in a solution of nitric acid and analysis by ICP-OES (Varian, Australia), and the results were reported in terms of MoO_3. It was found that on average, 0.1 mg of MoO_3 exist on every square centimeter geometric area of the electrodes.

Measurements by scanning potential microscopy (Dual Scope SPM, DME, Denmark) revealed round particles of molybdenum oxides of between 30 and 80 nm diameters.

Results and discussion

Cyclic voltammetry studies

Figure 1 presents cyclic voltammograms (CV) of ANMO/H_2SO_4 system for various concentrations of sulfuric acid and recorded at different potential sweep rates. The potential window is properly selected not to render ANMO unstable. Figure 2 compares the CVs recorded at the same potential sweep rate in different sulfuric acid solutions. Relatively poor capacitive behavior at high potential sweep rate and low acid concentration approaches to a fair, partially rectangular CV, as potential is swept slowly in higher acid concentrations. In fact, both the ionic charge transfer on the solution-electrode interface as well as the resistance related to the hydrogen inside the film should account for the kinetic limitation responsible for the deviation of the CVs from capacitive behavior [23]. Extending the cathodic end of the half-cycles tends to destroy the capacitive surface while hydrogen evolution accompanies. The redox processes responsible for the accumulation of charge is likely to be

$$MoO_x \times yH_2O + \delta H^+ + \delta\bar{e} \underset{\text{Discharge}}{\overset{\text{Charge}}{\rightleftarrows}} MoO_{x-\delta}(OH)_\delta \times yH_2O \quad (1)$$

while double-layer charging and diffusion of hydrogen ion (or else) from the surface to the interior of the active material (ANMO) certainly accompany reaction 1. This reaction resembling the origin of ruthenium oxide Faradaic capacitance [24] is in qualitative agreement with the CV findings. High acid concentration enhances charge accumulation but on the other hand favors instability and hydrogen evolution at less negative potentials.

Galvanostatic discharge curves

The capacitive behavior of a material can be estimated from charge/discharge follow:

$$SC\left(\mathbf{F\ g}^{-1}\right) = \frac{i(\mathrm{A}) \times \Delta t(\mathrm{s})}{\Delta E(\mathrm{V}) \times m(\mathrm{g})} \quad (2)$$

where i is the current, Δt is the discharge time, ΔE is the change in potential during the discharge process, and m is the mass of the active material. Figure 3 presents the discharge curves of the as-deposited molybdenum oxide between −0.2 and −0.45 V vs. Ag/AgCl at 0.1 mA cm^{-2} for different concentrations of H_2SO_4. Increasing the concentration of H_2SO_4, discharge time increases, which is related to more accumulated charge on the ANMO surface on the basis of the cyclic voltammetry results. Also, a sharp potential change is observed at initial stages of discharge, which is likely due to both IR drop and kinetic overpotential [25–27]. The assignments seem justified as upon increasing the acid concentration, the potential change diminishes on account of the increased conductivity of solution and more availability of protons for the Faradic process. On the other hand, when the Faradaic process Eq. 1 cannot provide the required charge to be withdrawn at the particular cell current, a kinetic resistance builds up.

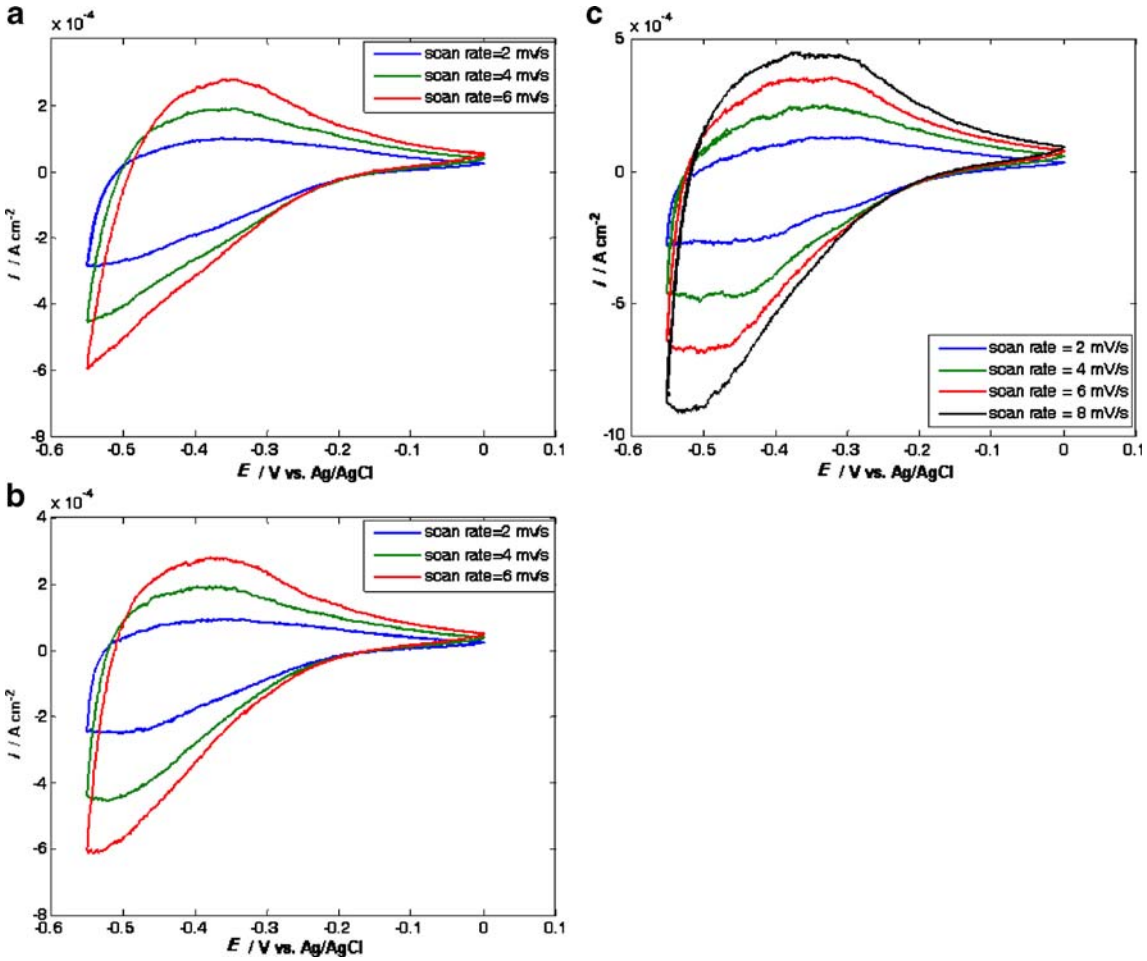

Fig. 1 Cyclic voltammograms of ANMO at different scan rates in **a** 0.005 M, **b** 0.010 M, and **c** 0.02 M H_2SO_4 solution

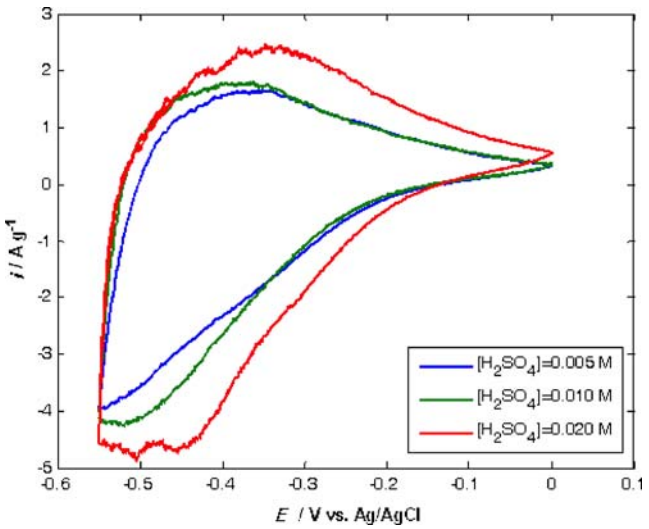

Fig. 2 Cyclic voltammograms of ANMO at scan rate of 4 mV/s in different concentrations of H_2SO_4

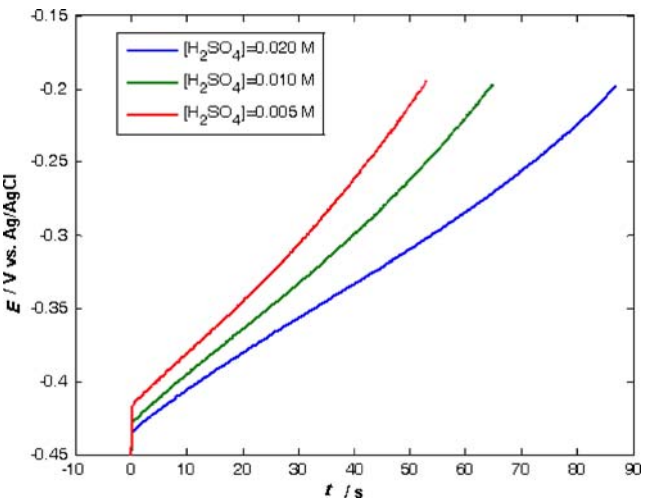

Fig. 3 Discharging curves of ANMO at 0.1 mA/cm^2 in different concentrations of H_2SO_4

Table 1 The discharge specific capacitance of ANMO at 0.1 mA/cm^2 cell current and different concentrations of H_2SO_4

$[H_2SO_4]$/M	Specific capacitance/F g^{-1}
0.005	347.4
0.010	467.0
0.020	650.1

The amount of the kinetic resistance is an evidence for disability of Faradaic process to supply charge at the required rate. In higher concentration of H_2SO_4, more hydrogen ions are available as a reagent for Faradaic reaction, and with regard to cyclic voltammetric studies, more accumulated charge exists to be withdrawn at the cell current and kinetic resistance thus decreases.

As Fig. 3 shows, the potential changes during discharging have two parts, a linear sharp change region and a mild nonlinear potential drop region [28], which runs the capacity of active electrodic materials. Due to this nonlinear change in potential vs. time, ΔE in Eq. 2 should be considered as an average potential for second region [25–27], which is calculated by:

$$\Delta E_{ave} = \frac{1}{\Delta t}\int_{t_1}^{t_2} E dt \tag{3}$$

Specific discharge capacitances have been calculated by using galvanic discharging curves (Fig. 3), and Eqs. 2 and 3 and have been shown in Table 1. As these data show, discharging capacitance enhances by increasing in concentration of H_2SO_4, which satisfies the cyclic voltammetric results.

Electrochemical impedance spectroscopy studies

The complex-plane impedance (Nyquist plots) and dependency of impedance magnitude, phase angle, and capacitance on frequency (Bode plots) for ANMO -0.35 V vs. Ag/AgCl in different concentration of H_2SO_4 have been presented in Fig. 4a–d. The capacitance was calculated from the

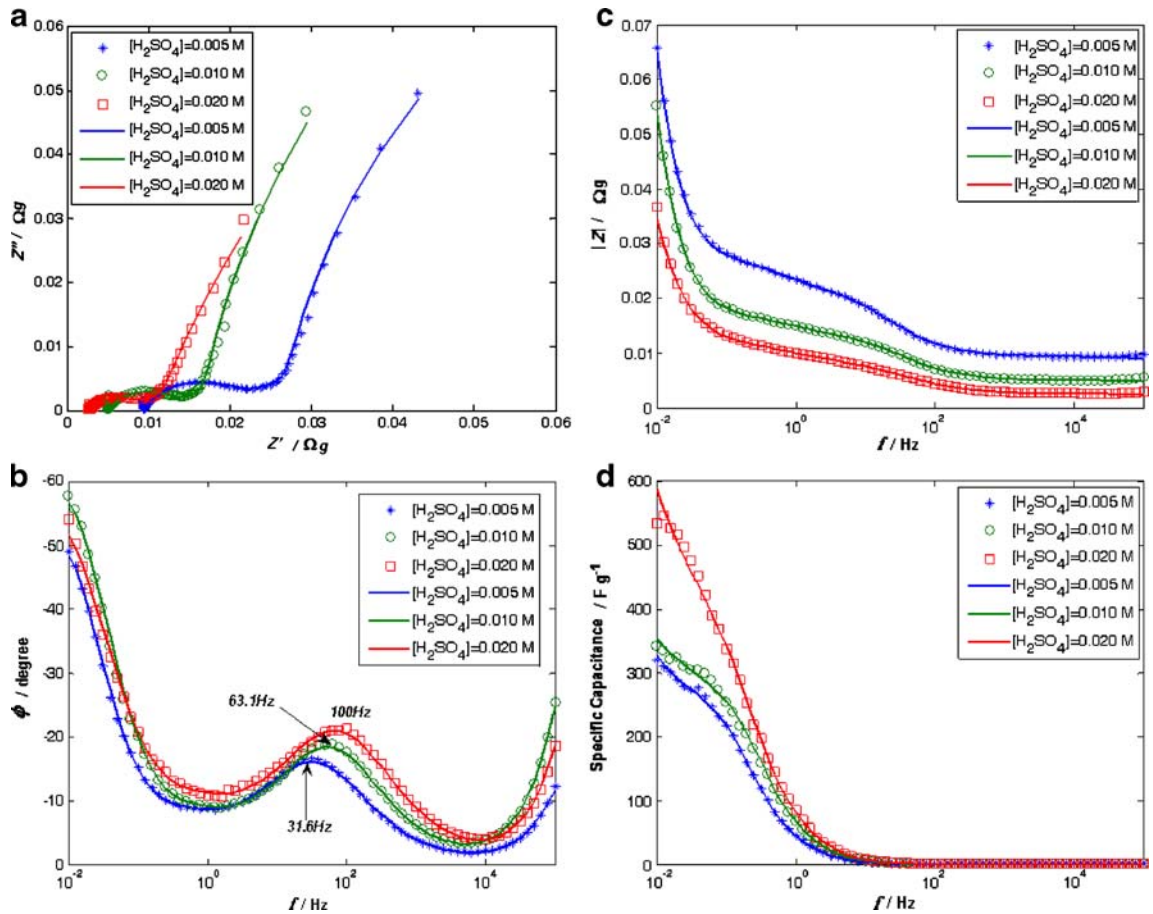

Fig. 4 The **a** Nyquist plots of ANMO in different concentrations of H_2SO_4 at −0.35 V vs. Ag/AgCl. Frequency dependence of the **b** phase angel; the characteristic knee frequency has been shown: **c** impedance magnitude and **d** capacitance. The *solid lines* represent the fitted data to the equivalent circuit in Fig. 5

Table 2 The capacity of ANMO at different concentration of H_2SO_4 at −0.35 V vs. Ag/AgCl

$[H_2SO_4]$/M	Specific capacitance/F g^{-1}
0.005	315
0.010	365
0.020	580

frequency dependency of the imaginary part of the impedance, Z″, through:

$$C = \frac{1}{2\pi f Z''} \tag{4}$$

The Nyquist plots (Fig. 4a) exhibit a squashed semicircle terminating to a line (slightly curved) with a slope close to 90°. The existing deviations from the straight line are related to nonideality of the capacitor (leaking capacitor). The knee frequency values have been shown in Fig. 4b. The knee frequency is the lower limit of the high frequency region of impedance spectrum, a region where $|Z|$ is weakly dependent on frequency (Fig. 4c) and the capacitance is near zero (Fig. 4d) [29]. At frequencies higher than the knee frequency, fast charge transfer processes, double-layer charging, etc. will dominate and slow Faradaic charge/discharge and mass transfer processes are thus ignored. The low frequency region is defined as the region where the Z–f plot possesses a slope close to −1 and $-90° < \phi < -45°$ in the f–ϕ plot. The near −1 slope shows that this region is typical of capacitive behavior. The frequency where $\phi = -45°$ is recognized as the frequency response to the ideal capacitor. At low frequency region ($f \leq f_{\phi=-45°}$), nonhomogeneous diffusion in the less accessible sites or leakage current may govern the impedance [29]. The range of frequencies between knee frequency and capacitor response frequency defines the medium frequency region where the kinetics of system is under diffusion control and distributed capacitance and resistance within the film (Warburg impedance) dominate the impedance. As Fig. 4b shows, by going to more concentrated solutions, the knee frequency increases. It means that double-layer charging occurs faster, or double-layer charging time constant becomes smaller. In fact, at a higher concentration of acid and at a fixed potential, more hydrogen ions are available to make the interface charged. On the other hand, double-layer charging time constant inversely depends to the conductivities of solution and the solid matrix [25], and both of these conductivities increase by increasing in concentration of acid. The argument is in accord with results of $f - |Z|$ plots (Fig. 4c). The argument is further supported by the diminished first semicircle and its shift to the lower limit of the real axis of the Nyquist plots. Also, by increasing in acid concentration, the semicircles become smaller more squashed, which imply that the double-layer capacitance increases, charge transfer resistance decreases, and more internal areas of the electrode is accessible. The phase angle behavior plots (Fig. 4b) show that the capacitor response frequency increases by increasing in concentration of acid, i.e. at higher concentrations, pseudo-capacitance is observed over a wider range of frequencies (Fig. 4d). Maximum capacitances, which are measured by impedance technique at −0.35 V vs. Ag/AgCl, have been collected in Table 2 for different solutions.

Finally, to have a better understanding of the parameters, which are important in impedance response of ANMO, we used the equivalent circuit shown in Fig. 5. This equivalent circuit has previously been employed by Sugimoto et al. [29] to investigate the response of hydrated ruthenium oxide in 10 M H_2SO_4.

The total impedance of equivalent circuit (Fig. 5) can be written as:

$$Z_{\text{total}} = R_s + \frac{1}{\frac{1}{Z_C} + \frac{1}{R_1 + Z_W} + \frac{1}{R_2 + \frac{1}{\frac{1}{R_3} + \frac{1}{Z_{CPE}}}}} \tag{5}$$

Where R_S is the solution resistance, Z_C is the double-layer impedance, and R_1 is the ohmic resistance accompanying mass transfer impedance, Z_W. R_2 is the charge transfer resistance through which pseudo-capacitance is charged/discharged, Z_{CPE} is the constant phase element signifying Faradic capacitance, and R_3 is the leakage resistance of the capacitor. This equivalent circuit fitted with the experimental data very well (solid lines in Fig. 4a–d), and some of the circuit parameters have been presented in Table 3.

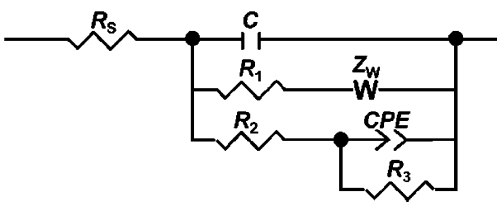

Fig. 5 The equivalent circuit used for fitting experimental results containing three parallel branches for double-layer capacitance, Warburg impedance, and a constant phase element signifying pseudo-capacitance

Table 3 Values of some of the equivalent circuit parameters at −0.35 V vs. Ag/AgCl in different concentrations of H_2SO_4

$[H_2SO_4]$/M	C_{dl}/μF g^{-1}	R_W/Ω g	R_{CT}/Ω g
0.005	646	0.0179	0.0191
0.010	573	0.0111	0.0151
0.020	929	0.0100	0.0091

Conclusion

The as-deposited nanostructured molybdenum oxide (ANMO) on stainless steel in acid solution shows capacitive behavior, which is enhanced by increasing the acid concentration. The leaky nature of the capacitor clearly appears in the Nyquist plots in the form of slightly curved capacitive lines. The instability of molybdenum oxide in acid solution acts as a limiting factor, which does not permit using high concentration of acid (>0.02 M) to achieve higher capacitances. Capacitance as high as 600 F g^{-1} has been measured.

References

1. Bailar JC, Emeléus HJ, Nyholm SR, Trotman-Dickenson AF (eds) (1973) Comprehensive inorganic chemistry vol 3. Pergamon, Oxford
2. Heracleous E, Lee AF, Vasalos IA, Lemonidou AA (2003) Catal Lett 88:47. doi:10.1023/A:1023534816277
3. Ferroni M, Guidi V, Martinelli G, Sacerdoti M, Nelli P, Sberveglieri G (1998) Sens Actuator B 48:285. doi:10.1016/S0925-4005(98) 00057-4
4. Imawan C, Steffes H, Solzbacher F, Obermeier E (2001) Sens Actuator B 77:346. doi:10.1016/S0925-4005(01) 00732-8
5. Granqvist CG (1995) Handbook of inorganic electrochromic materials. Elsevier, Amsterdam
6. Shembel E, Apostolova R, Nagirny V, Kirsanova I, Grebenkin P, Lytvyn P (2005) J Solid State Electrochem 9:96. doi:10.1007/s10008-004-0565-2
7. Yebka B, Julien C, Nazri GA (1999) Ionics 5:236. doi:10.1007/BF02375846
8. Christian PA, Carides JN, DiSalvo FJ, Waszczak V (1980) J Electrochem Soc 127:2315. doi:10.1149/1.2129404
9. McEvoy TM, Stevenson KJ (2003) Anal Chim Acta 496:39. doi:10.1016/j.aca.2002.10.001
10. McEvoy TM, Stevenson KJ (2004) J Mater Res 19:429. doi:10.1557/jmr.2004.19.2.429
11. McEvoy TM, Stevenson KJ, Hupp JT, Dang X (2003) Langmuir 19:4316. doi:10.1021/la027020u
12. Pathan HM, Min SK, Jung KD, Joo OS (2006) Electrochem Commun 8:273. doi:10.1016/j.elecom.2005.11.022
13. Guerfi A, Dao LH (1989) J Electrochem Soc 136:2435. doi:10.1149/1.2097408
14. Nagirnyi VM, Apostolova RD, Baskevich AS, Shembel EM (2004) Russ J Appl Chem 77:71. doi:10.1023/B:RJAC.0000024579.88110.c3
15. Więcek B, Twardoch U (2004) J Phys Chem Solids 65:263. doi:10.1016/j.jpcs.2003.08.022
16. Prasad KR, Koga K, Miura N (2004) Chem Mater 16:1845. doi:10.1021/cm0497576
17. Prasad KR, Miura N (2004) J Power Sources 135:354. doi:10.1016/j.jpowsour.2004.04.005
18. Prasad KR, Miura N (2004) Electrochem Commun 6:1004. doi:10.1016/j.elecom.2004.07.017
19. Prasad KR, Miura N (2004) Electrochem Commun 6:849. doi:10.1016/j.elecom.2004.06.009
20. Więcek B, Kępas-Suwara A (2007) Pol J Chem 81:129
21. Takasu Y, Ohnuma T, Sugimoto W, Murakami Y (1999) Electrochemistry 67:1187
22. Farsi H, Gobal F, Raissi H, Moghiminia S (2009) On the psuedocapacitive behavior of nanostructured molybdenum oxide. J Solid State Electrochem. doi:10.1007/s10008-009-830-5
23. García-Cañadas J, Mora-Seró I, Fabregat-Santiago F, Bisquert J, Garcia-Belmonte G (2004) J Electroanal Chem 565:329. doi:10.1016/j.jelechem.2003.10.027
24. Conway BE (1999) Electrochemical supercapacitors: scientific fundamentals and technological applications. Kluwer Academic/Plenum, New York
25. Lin C, Ritter JA, Popov BN, White RE (1999) J Electrochem Soc 146:3168. doi:10.1149/1.1392450
26. Farsi H, Gobal F (2007) J Solid State Electrochem 11:1085. doi:10.1007/s10008-006-0242-8
27. Farsi H, Gobal F (2009) J Solid State Electrochem 13:433. doi:10.1007/s10008-008-0576-5
28. Pico F, Ibañez J, Centeno TA, Pecharroman C, Rojas RM, Amarilla JM, Rojo JM (2006) Electrochim Acta 51:4693. doi:10.1016/j.electacta.2005.12.040
29. Sugimoto W, Iwata H, Yokoshima K, Murakami Y, Takasu Y (2005) J Phys Chem B 109:7330. doi:10.1021/jp044252o